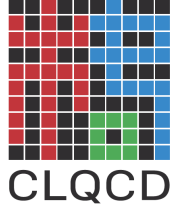


Impact of Dynamical Charm Quark and Mixed Action Effect on Light Hadron Masses and Decay Constants (CLQCD Collaboration)



Tong-Wei Lin,^{1,2,3} Zun-Xian Zhang,^{1,2,3} Mengchu Cai,^{2,*} Hai-Yang Du,^{2,4} Bolun Hu,⁵ Xiangyu Jiang,⁶ Xiao-Lan Meng,^{2,4} Ji-Hao Wang,^{2,4} Peng Sun,⁷ Yi-Bo Yang,^{2,4,1,8,†} and Dian-Jun Zhao⁹

¹*School of Fundamental Physics and Mathematical Sciences,*

Hangzhou Institute for Advanced Study, UCAS, Hangzhou 310024, China

²*Institute of Theoretical Physics, Chinese Academy of Sciences, Beijing 100190, China*

³*University of Chinese Academy of Sciences, Beijing 100049, China*

⁴*University of Chinese Academy of Sciences, School of Physical Sciences, Beijing 100049, China*

⁵*Computation-based Science and Technology Research Center,*

The Cyprus Institute, 20 Kavafi Str., Nicosia 2121, Cyprus

⁶*Department of Physics, Indiana University, Bloomington, Indiana 47405, USA*

⁷*Institute of Modern Physics, Chinese Academy of Sciences, Lanzhou, 730000, China*

⁸*International Centre for Theoretical Physics Asia-Pacific, Beijing/Hangzhou, China*

⁹*School of Science and Engineering, The Chinese University of Hong Kong, Shenzhen 518172, China*

(Dated: March 5, 2026)

We investigate the impact of including a dynamical charm quark on the properties of light hadrons. Our study uses gauge ensembles generated with the tadpole-improved Symanzik gauge action, comparing 2+1+1 flavor (HISQ fermion) ensembles at four lattice spacings to 2+1 flavor (clover fermion) ensembles at six lattice spacings. For the light and strange flavor observables, we employ the same tadpole-improved clover fermion action. From numerical results for light and strange quark masses, pion and kaon decay constants, and Ω baryon masses, we find that the values obtained after continuum, chiral, and infinite-volume extrapolations are consistent within uncertainties. Even though the mixed action setup can introduce additional discretization effects, our calculation shows evidences that those effects can cancel with the discretization error in the unitary setup, resulting in better convergence in the continuum extrapolation.

I. INTRODUCTION

The Standard Model of particle physics includes six flavors of quarks. Three of these—charm, bottom, and top—are heavier than the intrinsic scale of the strong interaction, $\Lambda_{\text{QCD}} \sim 300$ MeV. The other three—up, down, and strange—are lighter than Λ_{QCD} at a typical renormalization scale of 2 GeV in the $\overline{\text{MS}}$ scheme.

The three light flavors exhibit an approximate SU(3) flavor symmetry, with symmetry-breaking effects on the order of 10% for various observables. In contrast, the three heavy flavors are largely decoupled from light-hadron physics, a result supported by current lattice QCD averages in flavor physics [1].

A direct assessment of heavy flavors' impact on light-hadron physics is highly non-trivial. Introducing an additional flavor significantly alters the bare strong coupling

constant, which in turn modifies the bare quark masses that determine physical hadron masses. Furthermore, for widely used Wilson-like fermion formulations—such as Clover and twisted-mass fermions—these bare masses require additional parameter tuning due to additive mass renormalization from explicit chiral symmetry breaking. In contrast, mass tuning for staggered fermions is much simpler. However, calculations of hadronic observables with staggered fermions are complicated by ambiguities arising from taste-breaking effects.

This paradox can be resolved using a mixed-action approach: gauge ensembles are generated with dynamical staggered fermions across various flavor numbers, while hadronic observables are calculated using fermion actions without taste degree of freedom such as Clover. Although the leading-order low-energy constant for mixed-action effects has been shown to scale as roughly $\mathcal{O}(a^4)$ across a wide range of lattice spacings [2, 3], a systematic study of their impact on hadronic observables remains absent from the literature.

In this work, we compute light hadronic observables

* Corresponding author: caimengchu@itp.ac.cn

† Corresponding author: ybyang@itp.ac.cn

using clover valence fermions on dynamical 2+1+1-flavor HISQ fermion and Symanzik gauge ensembles spanning four lattice spacings, three pion masses, and several spatial volumes. Compared to results obtained using the 2+1 flavor ensembles using the same clover fermion and Symanzik gauge actions, we find that the discretization errors from this mixed-action setup are significantly reduced, with potential $\mathcal{O}(a^4)$ contributions remaining negligible within our statistical uncertainties. Finally, we update the predictions for low-energy constants from a previous 2+1 flavor CLQCD study [4], now with improved control over systematic uncertainties using the ensembles at three more lattice spacings.

II. SIMULATION SETUP

In this work, we use the 1-step stout link smeared (with smear size $\rho = 0.125$) clover valence fermion action [4, 5],

$$S_q(\tilde{m}) = \sum_x \left\{ \bar{\psi}(x + \eta\hat{\mu}a) \sum_{\mu=1,\dots,4,\eta=\pm} \frac{1 - \eta\gamma_\mu}{2} V_{\eta\mu}(x) + \psi(x) \left[- (4 + \tilde{m})\delta_{y,x} + \frac{c_{\text{sw}}}{2} \sigma^{\mu\nu} g_0 \sum_{\mu < \nu} F_{\mu\nu}^V \right] \right\} \psi(x), \quad (1)$$

where $c_{\text{sw}} = \frac{1}{v_0^3}$ with v_0 being the tadpole improved factor of the smeared gauge link V , and we use \tilde{O} for the dimensionless value of any quantity O .

The calculation are performed on two sets of the gauge ensembles: one set is the 2+1-flavor ensembles using the tadpole improved Symanzik gauge action and the same sea fermion action, and the other is the 2+1+1-flavor ones using using the same gauge action but the HISQ fermion action. The first set has been used in the previous CLQCD works (e.g., those for the basic parameter calibrations [4, 5]), and second set is generated recently and has been used for the determination of the mixed action effect in the valence-sea mixed pion mass [3].

The updated lattice spacing a [6], the dimensionless lattice volume $\tilde{L}^3 \times \tilde{T}$, and the finite-volume parameter $m_\pi L$ for the gauge ensembles generated with the clover fermion action are listed in Table I. For the ensembles marked with a superscript “*”, we generate new quark propagators and correlation functions; for the remaining ensembles, we reuse the data from previous CLQCD work [4].

Similar information for the newly generated gauge ensembles with the HISQ fermion action is provided in Table I. The strange and charm quark masses are tuned to their physical values for most ensembles. The exception is the c24P31s ensemble, for which we deliberately vary the quark masses to investigate mistuning effects. We have also generated three additional 2+1 flavor ensembles to isolate the impacts of the charm sea quark from those of the mixed-action setup, using the tree level Symanzik gauge action (x24P31), tadpole improved

TABLE I. Summary table on the lattice spacing, $m_\pi L$, $\tilde{L}^3 \times \tilde{T}$ and m_{π,η_s} (In units of MeV) of the CLQCD ensembles with Clover fermion. The ensembles with superscript * are newly generated after the previous CLQCD work [4].

Ensemble	a (fm)	$m_\pi L$	$\tilde{L}^3 \times \tilde{T}$	m_π (MeV)	m_{η_s} (MeV)
C24P34		4.37	$24^3 \times 64$	340.6(1.7)	749.2(0.7)
C24P29		3.75	$24^3 \times 72$	292.4(1.0)	658.5(0.6)
C32P29	0.10542(17)(62)	5.02	$32^3 \times 64$	293.4(0.8)	659.5(0.4)
C32P23		3.90	$32^3 \times 64$	228.1(1.2)	644.6(0.4)
C48P23		5.75	$48^3 \times 96$	224.3(1.2)	644.8(0.6)
C48P14		3.50	$48^3 \times 96$	136.5(1.7)	707.3(0.4)
E28P35*		4.42	$28^3 \times 64$	345.4(1.1)	710.7(1.0)
E32P29*	0.09013(25)(53)	4.17	$32^3 \times 64$	285.4(1.8)	698.2(0.9)
E32P22*		3.14	$32^3 \times 96$	215.1(2.2)	685.8(0.7)
F32P30		3.79	$32^3 \times 96$	301.0(1.2)	677.3(1.0)
F48P30		5.73	$48^3 \times 96$	303.5(0.7)	676.1(0.5)
F32P21	0.07760(07)(46)	2.65	$32^3 \times 64$	210.5(2.2)	660.1(0.9)
F48P21		3.93	$48^3 \times 96$	207.9(1.1)	663.7(0.6)
F64P14*		3.41	$64^3 \times 128$	135.6(1.2)	681.0(0.5)
G36P29*	0.06895(17)(41)	3.72	$36^3 \times 108$	295.7(1.1)	692.6(0.5)
H48P32	0.05235(11)(31)	4.03	$48^3 \times 144$	316.1(1.0)	690.6(0.7)
I64P31*	0.03761(08)(22)	3.81	$64^3 \times 128$	312.2(1.6)	671.4(1.3)

TABLE II. Summary table on the lattice spacing, $\tilde{L}^3 \times \tilde{T}$, $m_\pi L$ and m_{π,η_s,η_c} (In unit of MeV) of the CLQCD ensembles with HISQ fermion [3].

Ensemble	a (fm)	$\tilde{L}^3 \times \tilde{T}$	$m_\pi L$	m_π	m_{η_s}	m_{η_c}
c24P31s		$24^3 \times 48$	4.13	313(2)	745(3)	2.973(12)
c24P31		$24^3 \times 48$	4.07	309(2)	687(3)	2.972(12)
c32P31		$32^3 \times 48$	5.44	310(1)	686(3)	2.972(12)
c24P22	0.1084(4)	$24^3 \times 48$	2.94	223(2)	685(3)	2.970(12)
c32P22		$32^3 \times 48$	3.87	220(1)	684(3)	2.970(12)
c48P13		$48^3 \times 48$	3.53	134(1)	683(3)	2.970(12)
e32P31	0.0867(4)	$32^3 \times 64$	4.41	313(2)	694(3)	3.015(13)
g32P32		$32^3 \times 64$	3.65	317(3)	692(3)	2.981(13)
g48P31	0.0710(3)	$48^3 \times 64$	5.38	311(2)	691(3)	2.983(13)
h48P31	0.0473(3)	$48^3 \times 96$	3.60	313(3)	692(5)	2.947(19)
x24P31	0.1114(6)	$24^3 \times 48$	4.35	321(2)	711(4)	–
y24P31	0.1116(6)	$24^3 \times 48$	4.22	311(2)	688(4)	–
z24P31	0.1128(7)	$24^3 \times 48$	4.35	317(2)	704(4)	–

Symanzik gauge action (y24P31, the same as the previous 2+1-flavor CLQCD ensembles), and Iwasaki gauge action (z24P31).

Due to the non-zero critical quark mass \tilde{m}_{crit} required to vanish the pion mass in the Clover fermion formulation, a direct definition of the renormalized quark mass m_q^R from the bare parameter \tilde{m}_q^b is ambiguous and should be replaced by the PCAC quark mass extracted from pseudoscalar quarkonium correlation functions as [4, 5, 7]:

$$m_q^{\text{PC}} = \frac{m_{\text{PS}} \sum_{\vec{x}} \langle A_4(\vec{x}, t) P^\dagger(\vec{0}, 0) \rangle}{2 \sum_{\vec{x}} \langle P(\vec{x}, t) P^\dagger(\vec{0}, 0) \rangle} \Big|_{t \rightarrow \infty}, \quad (2)$$

with m_{PS} denoting the corresponding pseudoscalar mass, $A_\mu = \bar{\psi} \gamma_5 \gamma_\mu \psi$ and $P = \bar{\psi} \gamma_5 \psi$. The renormalized quark mass is then given by $m_q^R = (Z_A/Z_P) m_q^{\text{PC}}$.

We compute the renormalization constants Z_A/Z_V and Z_A/Z_P for the Clover action using amputated vertex functions in Landau gauge [4, 8]. These functions, $\Lambda_{\mathcal{O}}(\mu^{\text{RI}}) = S^{-1}(p_1)G_{\mathcal{O}}(p_1, p_2)S^{-1}(p_2)|_{p_1^2=p_2^2=(p_1-p_2)^2=(\mu^{\text{RI}})^2}$, are derived from the point source quark propagator $S(p_{1,2})$ and the operator correlator $G_{\mathcal{O}}(p_1, p_2)$ for an off-shell quark with momentum $p_{1,2}$.

In addition to the Z_V obtained from the vector current normalization of the hadron matrix element, the ratio Z_A/Z_V , is obtained from that of the vertex functions,

$$\frac{Z_A}{Z_V} = \frac{\frac{1}{48}\text{Tr}[\Lambda_V(\mu^{\text{RI}})\gamma_\mu]}{\frac{1}{48}\text{Tr}[\Lambda_A^\mu(\mu^{\text{RI}})\gamma_\mu\gamma_5]}, \quad (3)$$

and the μ^{RI} dependence in the right hand side should cancel between denominator and numerator. Including this correction is essential for obtaining accurate values of $f_{\pi,K}$ after continuum extrapolation [4]. For the PCAC mass renormalization, we evaluate $Z_A/Z_P(\mu^{\text{RI}})$ at the RI/MOM scale μ [8],

$$\frac{Z_A}{Z_P(\mu)} = \frac{\frac{1}{12}\text{Tr}[\Lambda_P(\mu^{\text{RI}})\gamma_5]}{\frac{1}{48}\text{Tr}[\Lambda_A^\mu(\mu^{\text{RI}})\gamma_\mu\gamma_5]} \Big|_{p^2=\mu^2}, \quad (4)$$

followed by the chiral extrapolation with Goldstone pole subtracted [9], and also perturbative matching to the $\overline{\text{MS}}$ scheme 2 GeV [10].

For the hadronic observable, we generate quark propagators using a Coulomb gauge-fixed wall source at multiple time slices for a range of quark masses around the unitary light and strange quark masses. The PCAC quark masses, as well as the masses and decay constants of the pseudoscalar mesons, are then extracted through a joint fit of correlation functions constructed from different interpolating fields, following the methodology detailed in previous CLQCD works [4, 5].

In the light quark region, the PCAC quark mass \tilde{m}^{PC} depends on the bare quark mass linearly,

$$\begin{aligned} \tilde{m}^{\text{PC}} &= k_m(\tilde{m}^{\text{b}} - \tilde{m}_{\text{crit}}) \\ &= k_m^{\text{tad}}(\tilde{m}^{\text{b,tad}} - \tilde{m}_{\text{crit}}^{\text{tad}}), \end{aligned} \quad (5)$$

where $\tilde{m}_q^{\text{b,tad}} = \frac{4+\tilde{m}_q^{\text{b}}}{v_0} - 4$ is the tadpole improved bare quark mass. The fit parameters k^{tad} and $\tilde{m}_{\text{crit}}^{\text{tad}}$ for the ensembles with $m_\pi \sim 0.3$ GeV are collected in Table III. We also list the values of $\tilde{m}_{\text{crit}} = (4 + \tilde{m}_{\text{crit}}^{\text{tad}})v_0 - 4$ and $m_{\text{crit}}^{\text{tad}} = \tilde{m}_{\text{crit}}^{\text{tad}}/a$ for comparison.

As $m^{\text{PC}} \propto m_\pi^2$, the critical mass $m_{\text{crit}} \equiv \tilde{m}_{\text{crit}}/a$ measures explicit chiral symmetry breaking in the clover action. Despite an inherent $\mathcal{O}(\alpha_s/a)$ power divergence from the Wilson term, the nearly linear scaling of $\tilde{m}_{\text{crit}}^{\text{tad}}$ with a —and thus the mild dependence of $m_{\text{crit}}^{\text{tad}}$ —shows this divergence is strongly suppressed under full tadpole improvement (see Table III).

Table III also shows that $m_{\text{crit}}^{\text{tad}}$ is $\sim 40\%$ smaller on the 2+1+1 HISQ ensembles than on the 2+1 clover ensembles. Since a comparable reduction is seen on the 2+1

TABLE III. Summary of clover valence fermion mass parameters for the Clover and HISQ ensembles with $m_\pi \sim 0.3$ GeV at different lattice spacings. The table lists the slopes between the PCAC quark mass and the tadpole-improved bare quark mass, as well as the critical quark masses (in the original definition of fermion action, tadpole improved value $\tilde{m}_{\text{crit}}^{\text{tad}}$ and the associated dimensionful mass $m_{\text{crit}}^{\text{tad}}$).

	a (fm)	k_m^{tad}	\tilde{m}_{crit}	$\tilde{m}_{\text{crit}}^{\text{tad}}$	$m_{\text{crit}}^{\text{tad}}$ (GeV)
2+1 Clover sea	0.105	0.841(1)	-0.28571(3)	-0.09619(4)	-0.180(1)
	0.090	0.878(1)	-0.25753(5)	-0.07918(6)	-0.173(1)
	0.078	0.914(2)	-0.23546(4)	-0.06618(4)	-0.168(1)
	0.069	0.934(1)	-0.21982(2)	-0.05785(2)	-0.166(1)
	0.052	0.973(1)	-0.18882(1)	-0.04294(1)	-0.162(1)
0.038	0.998(1)	-0.15940(1)	-0.03119(1)	-0.164(1)	
2+1 HISQ sea	0.112	0.937(2)	-0.21379(9)	-0.06548(9)	-0.1158(2)
	0.108	0.947(2)	-0.20403(7)	-0.06056(8)	-0.1102(1)
2+1+1 HISQ sea	0.087	0.971(1)	-0.17179(4)	-0.04445(4)	-0.1012(1)
	0.071	0.984(2)	-0.15141(4)	-0.03520(5)	-0.0979(1)
	0.047	1.003(1)	-0.12081(1)	-0.02302(1)	-0.0961(1)

HISQ ensemble, we conclude the effect is due mainly to the difference between HISQ and clover quark actions in the gauge configurations, not the dynamical charm quark loop.

Finally, we also observe a significantly weaker lattice spacing dependence for the parameter k_m^{tad} on the HISQ ensembles. This feature would relate to similar reduction in the discretization errors for hadronic observables, a point that will be addressed in the subsequent discussion.

Using propagators with a partially quenched valence quark mass m_l^v on gauge ensembles with a light sea quark mass m_l^s , the partially quenched chiral perturbation theory (PQ χ PT) suggests the following ansatz for the pion mass and decay constant [4, 11]:

$$\begin{aligned} m_{\pi,\text{vv}}^2 &= \Lambda_\chi^2 2y_v \left\{ 1 + \frac{2}{N_f} [(2y_v - y_s)\ln(2y_v) + (y_v - y_s)] \right. \\ &\quad \left. + 2y_v(2\alpha_8 - \alpha_5) + 2y_s N_f(2\alpha_6 - \alpha_4) \right\} \\ &\quad \times [1 + c_L^\pi e^{-m_\pi L} + c_s^\pi (m_{\eta_s}^2 - m_{\eta_s,\text{phys}}^2)] \\ &\quad \times (1 + c_{a^2}^\pi a^2), \end{aligned} \quad (6)$$

$$\begin{aligned} F_{\pi,\text{vv}} &= F \left(1 - \frac{N_f}{2} (y_v + y_s)\ln(y_v + y_s) + y_v\alpha_5 + y_s N_f \alpha_4 \right) \\ &\quad \times [1 + d_{L,s}^\pi e^{-m_\pi L} + d_s^\pi (m_{\eta_s}^2 - m_{\eta_s,\text{phys}}^2)] \\ &\quad \times (1 + d_{a^2}^\pi a \log(u_0(a)) + d_{a^2}^\pi a^2) \end{aligned} \quad (7)$$

where $N_f = 2$ is the number of light flavors, $\Lambda_\chi = 4\pi F$ is the intrinsic scale of χ PT with F being the pion decay constant in the chiral limit, and $y_v/y_s = \frac{\Sigma m_l^{v/s}}{F^2 \Lambda_\chi^2}$ is the dimensionless expansion parameter of χ PT. Here, $\Sigma \equiv -\langle \bar{q}q \rangle_{m_l \rightarrow 0}$ denotes the chiral condensate in the $N_f = 2$ chiral limit, and $\alpha_{4,5,6,8}$ are the next-to-leading-order (NLO) low-energy constants. Additional parameters $c_{L,s}^\pi$ and d_{L,s,a^2}^π are introduced to parameterize corrections from finite volume, an unphysical strange-

quark mass, and finite lattice spacing. We further introduce the $d_{a\alpha_s}^\pi$ term in the f_π (and also $d_{a\alpha_s}^K$ in f_K) to capture the residual $a\alpha_s$ correction after the $\mathcal{O}(m_q a)$ effect is eliminated using the quark mass dependent vector current normalization [5], and the value of α_s is approximated using the relation $\alpha_s^{u_0} \equiv -\frac{4}{3.06839} \log u_0$ for the Symanzik gauge action [3, 12]. The m_π and f_π with unitary valence and sea quark masses $y = y_v = y_s$ have another widely used parameterization,

$$m_\pi^2 = \Lambda_\chi^2 2y [1 + y (\ln \frac{2y\Lambda_\chi^2}{m_{\pi,\text{phys}}^2} - \ell_3) + \mathcal{O}(y^2)], \quad (8)$$

$$F_\pi = F [1 - 2y (\ln \frac{2y\Lambda_\chi^2}{m_{\pi,\text{phys}}^2} - \ell_4) + \mathcal{O}(y^2)]. \quad (9)$$

where $\ell_{3,4}$ is related to $\alpha_{4,5,6,8}$ by

$$\begin{aligned} \ell_3 &= \ln \frac{\Lambda_\chi^2}{m_{\pi,\text{phys}}^2} - 2[(2\alpha_8 - \alpha_5) + 2(2\alpha_6 - \alpha_4)], \\ \ell_4 &= \ln \frac{\Lambda_\chi^2}{m_{\pi,\text{phys}}^2} + \frac{1}{2}(\alpha_5 + 2\alpha_4). \end{aligned} \quad (10)$$

Similarly, we fit the partially quenched Kaon masses and decay constants on all the ensembles using the following form proposed in recent works [4, 13],

$$\begin{aligned} m_K^2(m_l^v, m_l^s, m_s^v, m_s^s, a, 1/L) \\ = (b_s^v m_s^v + b_s^s m_s^s + b_l^v m_l^v + b_l^s m_l^s) \\ \times [1 + c_l^K m_l^v + c_{a^2}^K a^2 + c_L^K \exp(-m_\pi L)], \end{aligned} \quad (11)$$

$$\begin{aligned} f_K(m_l^v, m_l^s, m_s^v, m_s^s, a, 1/L) \\ = (f_0 + df_s^v m_s^v + df_s^s m_s^s + df_l^v m_l^v + df_l^s m_l^s) \\ \times [1 + d_{a\alpha_s}^K a \log(u_0(a)) + d_{a^2}^K a^2 + d_L^K \exp(-m_\pi L)]. \end{aligned} \quad (12)$$

The masses of the ϕ and Ω hadrons—which contain only valence strange quarks—are fitted using following empirical ansatz,

$$\begin{aligned} m_{H=\phi/\Omega}(m_l^s, m_s^v, m_s^s, a, 1/L) &= (m_H^{\text{phys}} \\ &+ \sum_{m_i=m_\pi^{\text{sea}}, m_{\eta_s}^{\text{val/sea}}} c_i^H (m_i^2 - m_{i,\text{phys}}^2)) \\ &\times [1 + c_{a^2}^H a^2 + c_L^H \exp(-m_\pi L)]. \end{aligned} \quad (13)$$

III. RESULTS

In this work, computations on the HISQ ensembles are performed using 50 configurations per ensemble, with 8 Coulomb wall source propagators generated on each configuration. Using a valence strange-quark mass tuned to the physical value via $m_{\eta_s}^{\text{phys}} = 689.89(49)$ MeV [14], we compute the masses m_ϕ and m_Ω on $N_f = 2 + 1 + 1$ ensembles at four lattice spacings and various light-quark masses. The results, shown as green circles (labeled

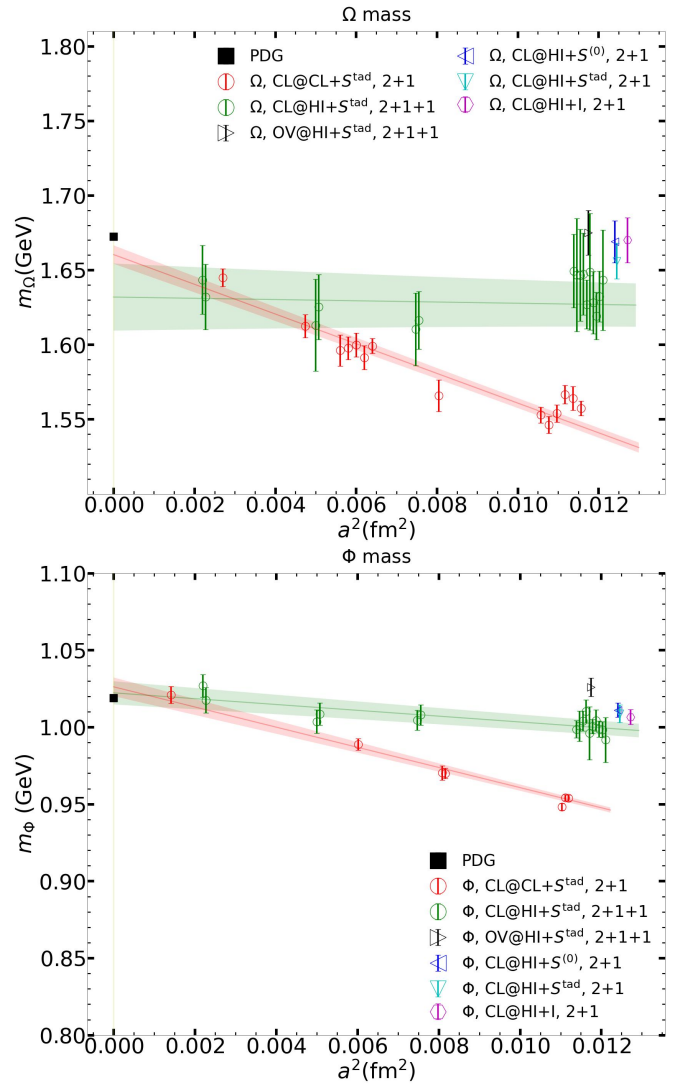


FIG. 1. Lattice spacing dependence of the m_ϕ (upper panel) and m_Ω using the valence strange quark mass tuned to $m_{\eta_s}^{\text{phys}} = 689.89(49)$ MeV .

CL@HI) in Fig. 1, are compared with analogous results from $N_f = 2 + 1$ ensembles using a unitary clover action [15] (red points, labeled CL@CL). Despite the relatively larger uncertainties in the CL@HI results, the discretization errors for both m_ϕ and m_Ω are significantly smaller than those in the CL@CL case.

To isolate the effect of a dynamical charm sea, we performed similar calculations on three $N_f = 2 + 1$ HISQ ensembles (x/y/z24P31) at a comparable pion mass and lattice spacing ($a \sim 0.11$ fm) but with different gauge actions. All three results agree well with each other and with those from the $N_f = 2 + 1 + 1$ ensembles. This indicates that the additional discretization error introduced by the valence-sea fermion mismatch can partially cancel the error inherent to the valence fermion action itself, leading to a reduced total discretization error—an effect that appears insensitive to the choice of gauge action or

the inclusion of a charm sea.

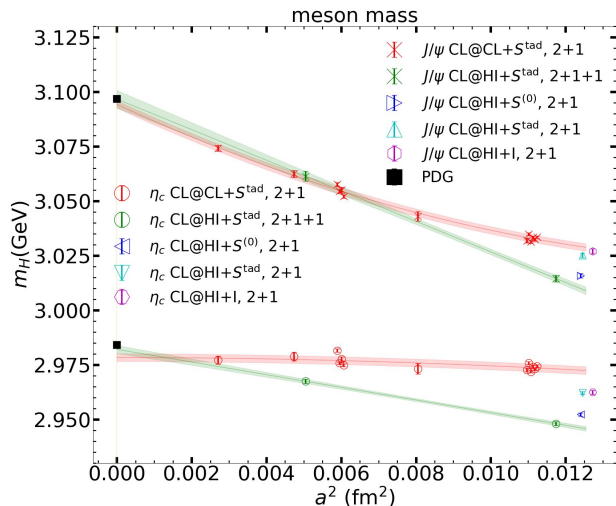


FIG. 2. Lattice spacing dependence of the charmonium masses m_{η_c} and $m_{J/\psi}$ using the valence charm quark mass tuned to the physical m_{D_s} .

Separately, using a valence charm-quark mass tuned to the QED-correction-subtracted $m_{D_s} = 1966.7(1.5)$ MeV, we compute the S-wave charmonium masses m_{η_c} and $m_{J/\psi}$ on the $N_f = 2+1+1$ ensembles c24P31 and g32P32 at two lattice spacings with $m_\pi \sim 310$ MeV. These results are shown as green crosses and circles (CL@HI) in Fig. 2. Compared to the corresponding unitary clover ($N_f = 2+1$) results [5] (red points, CL@CL), the clover-on-HISQ data exhibit a larger discretization error for m_{η_c} but a smaller a^4 correction for $m_{J/\psi}$, assuming the continuum limits agree with experiment.

To investigate the charm-sea effect here, we repeated the calculation on three $N_f = 2+1$ HISQ ensembles (x/y/z24P31) at similar parameters. On ensemble y24P31, which uses the same tadpole-improved Symanzik gauge action as our main sets, $m_{J/\psi}$ agrees with the unitary-clover results, while m_{η_c} is lower, producing a hyperfine splitting $\Delta_{\text{HFS}}^c \equiv m_{J/\psi} - m_{\eta_c}$ similar to the $N_f = 2+1+1$ case. Results on z24P31 (Iwasaki gauge action) are comparable. In contrast, x24P31 (tree-level Symanzik action) yields significantly different individual masses, though Δ_{HFS}^c remains statistically consistent across all HISQ ensembles, regardless of gauge action or charm sea.

We therefore conclude that the discretization of light-fermion loops in the gauge ensemble has a significant impact on charmonium mass discretization errors. Meanwhile, given the much higher statistical precision achievable in the charm sector, the effects of the dynamical charm sea and the choice of gauge action are also non-negligible.

Predictions for light meson masses and decay constants require non-perturbative renormalization and therefore

introduce additional systematic uncertainties. In the previous CLQCD study [4], the central values in the $\overline{\text{MS}}$ scheme were obtained via the RI/MOM scheme, and the difference between the RI/MOM and SMOM results was taken as a systematic uncertainty. Benefiting from additional data at three new lattice spacings, we now incorporate an $\mathcal{O}(a\alpha_s)$ term in the continuum extrapolation, together with a quark-mass-dependent vector current normalization [5], which removes the $\mathcal{O}(m_q a)$ correction.

Our final predictions—including quark masses, low-energy constants, pion and kaon decay constants, and other fit parameters—are summarized in Table IV for both the $N_f = 2+1$ unitary clover (CL@CL) setup and the $N_f = 2+1+1$ mixed-action (CL@HI) setup. For comparison, the table also includes results from the previous CLQCD study [4], which used a subset of the $N_f = 2+1$ CLQCD ensembles at three lattice spacings.

As shown in Table IV, the updated $N_f = 2+1$ CL@CL results are consistent with those from Ref. [4] when the same intermediate renormalization scheme (MOM or SMOM) is used. In certain cases, the uncertainties are slightly larger due to the inclusion of the $a\alpha_s$ term, although the coefficient of the $a\alpha_s$ dependence in f_π exceeds 2σ by only a small margin. The values of m_l , m_s , f_π , and f_K obtained via the MOM scheme still deviate from those via the SMOM scheme by approximately 2σ , while the scheme-independent ratios m_s/m_l and f_K/f_π remain consistent within uncertainties.

For the $N_f = 2+1+1$ CL@HI results, the uncertainties are larger due to limited statistics. However, the discretization errors in f_π and f_K are significantly smaller, regardless of whether the MOM or SMOM scheme is used for renormalization. Consequently, the consistency between the results obtained with the two schemes is better than in the CL@CL case, although the impact of the larger statistical uncertainties warrants further investigation. This observation provides additional evidence that our mixed-action setup can also suppress discretization errors at the level of hadronic matrix elements.

The FLAG averages for both the 2+1 and 2+1+1 cases [1, 4, 13, 16–72] are also listed in Table IV for comparison.

After correcting for unphysical strange- and light-quark masses using the parameters from the joint fit, we present the corrected kaon decay constant f_K through the RI/MOM renormalization, as a function of a^2 in Fig. 3. The comparison between the $N_f = 2+1+1$ (CL@HI) and $N_f = 2+1$ (CL@CL) cases illustrates the suppression of discretization errors in hadronic matrix elements for the CL@HI setup.

IV. SUMMARY

In Summary, we studied the feature and discretization errors of using the tadpole improved clover fermion with stout smeared gauge link, on the 2+1+1 flavor HISQ fermion ensembles. Compared to the similar calcula-

TABLE IV. Summary of our determination on quark masses at $\overline{MS}(2\text{GeV})$ and the other quantities, with comparison with FLAG [1, 4, 13, 16–72] and/or PDG [73].

	CL@CL, 2+1					HI@CL, 2+1+1		
	MOM		SMOM		FLAG/PDG	RIMOM	RISMOM	FLAG/PDG
	Ref. [4]	This work	Ref. [4]	This work				
m_l (MeV)	3.60(11)	3.52(08)	3.45(05)	3.34(04)	3.387(39)	3.46(17)	3.46(09)	3.427(51)
m_s (MeV)	98.8(2.9)	97.2(1.7)	94.1(1.2)	92.7(1.0)	92.4(1.0)	97.1(5.0)	96.7(1.9)	93.46(58)
m_s/m_l	27.47(30)	27.65(73)	27.28(22)	27.80(28)	27.42(12)	28.1(2.0)	28.0(0.7)	27.227(81)
$\Sigma^{1/3}$ (MeV)	268.6(3.6)	269.0(2.9)	269.3(1.8)	271.4(2.0)	272(5)	275.7(6.5)	275.5(4.4)	286(23)
F (MeV)	86.6(0.7)	85.8(0.9)	85.1(0.6)	84.7(0.8)		87.9(2.3)	88.1(2.2)	
l_3	2.43(54)	2.57(35)	2.49(23)	2.53(13)	3.07(64)	3.56(97)	2.95(54)	3.53(26)
l_4	4.32(08)	4.25(05)	4.23(05)	4.19(03)	4.02(45)	4.02(13)	3.94(13)	4.73(10)
c_s^π (GeV ²)		0.06(11)		0.03(04)		-0.120(280)	-0.003(137)	
d_s^π (GeV ²)		0.204(31)		0.217(30)		0.16(10)	0.16(10)	
b_s^V (GeV)		2.333(75)		2.505(35)		2.59(23)	2.45(11)	
b_s^S (GeV)		0.077(81)		0.024(29)		-0.18(30)	-0.03(12)	
b_l^V (GeV)		2.26(39)		2.17(15)		4.3(1.7)	1.6(0.8)	
b_l^S (GeV)		0.47(13)		0.55(06)		0.34(47)	0.49(18)	
df_s^V		0.1897(58)		0.1957(48)		0.165(24)	0.173(19)	
df_s^S		0.066(27)		0.091(22)		0.047(63)	0.058(56)	
df_l^V		0.239(16)		0.239(15)		0.133(59)	0.135(55)	
df_l^S		0.405(30)		0.413(26)		0.308(78)	0.245(63)	
c_l^K (GeV ⁻¹)		0.9(1.2)		1.1(0.5)		-5.2(5.0)	3.9(3.0)	
$c_{a_2}^\pi$ (fm ⁻²)		-0.2(3.1)		-1.4(0.7)		1.70(2.40)	0.03(1.04)	
$d_{a_2}^\pi$ (fm ⁻²)		-3.23(78)		-6.94(46)		0.63(69)	-2.24(60)	
$d_{a\alpha_s}^\pi$ (fm ⁻¹)		0.55(28)		0.82(28)		-0.130(93)	-0.109(96)	
$c_{a_2}^K$ (fm ⁻²)		-0.5(3.2)		-1.2(0.6)		0.9(2.0)	-0.4(0.9)	
$d_{a_2}^K$ (fm ⁻²)		-4.5(1.1)		-7.6(0.9)		-0.15(68)	-3.14(52)	
$d_{a\alpha_s}^K$ (fm ⁻¹)		1.37(81)		0.99(78)		-0.18(18)	-0.12(17)	
c_L^π		0.61(31)		0.48(18)		0.69(47)	0.85(36)	
d_L^π		-4.51(54)		-0.60(12)		-0.40(21)	-0.44(21)	
c_L^K		0.16(16)		0.21(07)		-0.04(37)	0.32(18)	
d_L^K		-0.299(56)		-0.301(50)		-0.08(15)	-0.09(13)	
f_π (MeV)	130.7(0.9)	129.5(1.1)	128.6(0.8)	127.9(1.0)	130.2(0.8)	131.7(2.7)	131.7(2.7)	
f_{K^\pm} (MeV)	155.6(0.8)	157.5(1.1)	152.9(0.7)	155.1(1.1)	155.7(0.7)	157.2(2.2)	157.1(2.1)	155.7(0.3)
F_π/F	1.0675(19)	1.0672(18)	1.0683(15)	1.0678(16)	1.0620(70)	1.0593(59)	1.0567(58)	1.0770(30)
f_K/f_π	1.1907(76)	1.2162(94)	1.1890(74)	1.2132(95)	1.1916(34)	1.194(20)	1.193(21)	1.1934(19)

tion on the unitary 2+1 flavor clover fermion ensembles, the discretization error of the hadronic observable likes $f_{\pi,K}$ and $m_{\phi,\Omega}$ are significantly suppressed. Thus even though the mixed action setup can introduce additional discretization effects, our calculation shows evidences that those effects can cancel with the discretization error in the unitary setup and resulting better control on the systematic uncertainty from the continuum extrapolation, using the combination of the stout smeared clover fermion on the HISQ sea with tadpole improved Symanzik gauge action.

Our investigation at $a \sim 0.1$ fm further indicates that, within current statistical uncertainties, the inclusion of a dynamical charm quark sea does not alter low-energy hadronic physics. However, given the significantly smaller statistical errors achievable in charm-physics observable, such inclusion can modify the coefficients of the corresponding discretization errors. Furthermore, we find that hadron masses computed using the tadpole-improved Symanzik gauge action are consis-

tent with those from the Iwasaki gauge action, agreeing well within uncertainties. Future studies at finer lattice spacings or with different valence fermion actions would provide more stringent tests of these findings.

ACKNOWLEDGEMENT

We thank the CLQCD collaborations for providing us their gauge configurations with dynamical fermions [3–5], which are generated on Advanced Computing East China Sub-center, HPC Cluster of ITP-CAS, IHEP-CAS and CSNS-CAS, ORISE Supercomputer, the Southern Nuclear Science Computing Center(SNSC) and the Siyuan-1 cluster supported by the Center for High Performance Computing at Shanghai Jiao Tong University. We thank Ying Chen, Hengtong Ding, Xu Feng, Chuan Liu, Li-uming Liu, Wei Wang and the other CLQCD members for valuable comments and suggestions. The calculations were performed using the PyQUDA package [74] with

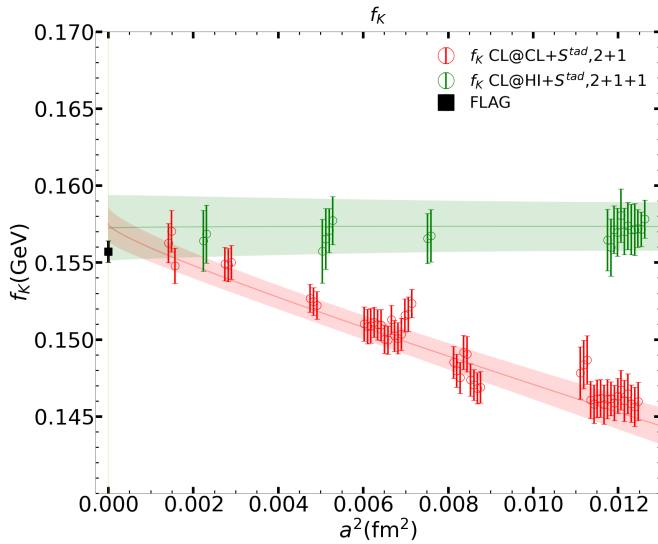


FIG. 3. Lattice spacing dependence of the f_K with the impacts from the unphysical strange and light quark masses corrected using the parameters obtained from the joint fit.

QUADA [75–77] through HIP programming model [78]. The numerical calculation were carried out on the Advanced Computing East China Sub-center, ORISE Supercomputer and HPC Cluster of ITP-CAS. This work is supported in part by National Key R&D Program of China No.2024YFE0109800, NSFC grants No. 12525504, 12435002, 12293060, 12293062, 12293061, 12293065 and 12447101, the Strategic Priority Research Program of Chinese Academy of Sciences, Grant No. YSBR-101.

-
- [1] Y. Aoki *et al.* (Flavour Lattice Averaging Group (FLAG)), FLAG review 2024, *Phys. Rev. D* **113**, 014508 (2026), [arXiv:2411.04268 \[hep-lat\]](#).
- [2] D.-J. Zhao, G. Wang, F. He, L. Jin, P. Sun, Y.-B. Yang, and K. Zhang (χ QCD), Distance between various discretized fermion actions, *Phys. Rev. D* **107**, L091501 (2023), [arXiv:2207.14132 \[hep-lat\]](#).
- [3] Z.-X. Zhang, M. Cai, B. Hu, X. Jiang, Y.-B. Yang, and D.-J. Zhao, Comparison of the mixed-fermion-action Effects using different fermion and gauge actions with 2+1 and 2+1+1 flavors, (2025), [arXiv:2512.19265 \[hep-lat\]](#).
- [4] Z.-C. Hu *et al.* (CLQCD), Quark masses and low-energy constants in the continuum from the tadpole-improved clover ensembles, *Phys. Rev. D* **109**, 054507 (2024), [arXiv:2310.00814 \[hep-lat\]](#).
- [5] H.-Y. Du *et al.* (CLQCD), Charmed meson masses and decay constants in the continuum limit from the tadpole improved clover ensembles, *Phys. Rev. D* **111**, 054504 (2025), [arXiv:2408.03548 \[hep-lat\]](#).
- [6] M. C. Cai *et al.* (CLQCD), Bottom physics, in preparation.
- [7] T. Ishikawa *et al.* (JLQCD), Light quark masses from unquenched lattice QCD, *Phys. Rev. D* **78**, 011502 (2008), [arXiv:0704.1937 \[hep-lat\]](#).
- [8] G. Martinelli, C. Pittori, C. T. Sachrajda, M. Testa, and A. Vladikas, A general method for non-perturbative renormalization of lattice operators, *Nucl. Phys. B* **445**, 81 (1995), [arXiv:hep-lat/9411010](#).
- [9] Z. Liu, Y. Chen, S.-J. Dong, M. Glatzmaier, M. Gong, A. Li, K.-F. Liu, Y.-B. Yang, and J.-B. Zhang (χ QCD), Nonperturbative renormalization of overlap quark bilinears on 2+1-flavor domain wall fermion configurations, *Phys. Rev. D* **90**, 034505 (2014), [arXiv:1312.7628 \[hep-lat\]](#).
- [10] J. A. Gracey, Five loop anomalous dimension of non-singlet quark currents in the $\overline{\text{RI}}'$ scheme, *Eur. Phys. J. C* **83**, 181 (2023), [arXiv:2210.12420 \[hep-ph\]](#).
- [11] S. R. Sharpe, Enhanced chiral logarithms in partially quenched QCD, *Phys. Rev. D* **56**, 7052 (1997), [Erratum: *Phys. Rev. D* 62, 099901 (2000)], [arXiv:hep-lat/9707018](#).
- [12] M. G. Alford, W. Dimm, G. P. Lepage, G. Hockney, and P. B. Mackenzie, Lattice QCD on small computers, *Phys. Lett. B* **361**, 87 (1995), [arXiv:hep-lat/9507010](#).
- [13] C. Alexandrou *et al.* (Extended Twisted Mass), Quark masses using twisted-mass fermion gauge ensembles, *Phys. Rev. D* **104**, 074515 (2021), [arXiv:2104.13408 \[hep-lat\]](#).
- [14] S. Borsanyi *et al.*, Leading hadronic contribution to the muon magnetic moment from lattice QCD, *Nature* **593**, 51 (2021), [arXiv:2002.12347 \[hep-lat\]](#).
- [15] B. Hu, H. Du, X. Jiang, K.-F. Liu, P. Sun, and Y.-B. Yang, Unveiling the Strong Interaction origin of Baryon Masses with Lattice QCD, (2024), [arXiv:2411.18402 \[hep-lat\]](#).
- [16] Y. Aoki *et al.* (Flavour Lattice Averaging Group (FLAG)), FLAG Review 2021, *Eur. Phys. J. C* **82**, 869 (2022), [arXiv:2111.09849 \[hep-lat\]](#).
- [17] R. Arthur *et al.* (RBC, UKQCD), Domain Wall QCD with Near-Physical Pions, *Phys. Rev. D* **87**, 094514 (2013), [arXiv:1208.4412 \[hep-lat\]](#).
- [18] M. Bruno, I. Campos, P. Fritzsche, J. Koponen, C. Pena, D. Preti, A. Ramos, and A. Vladikas (ALPHA), Light quark masses in $N_f = 2 + 1$ lattice QCD with Wilson fermions, *Eur. Phys. J. C* **80**, 169 (2020), [arXiv:1911.08025 \[hep-lat\]](#).
- [19] T. Blum *et al.* (RBC, UKQCD), Domain wall QCD with physical quark masses, *Phys. Rev. D* **93**, 074505 (2016), [arXiv:1411.7017 \[hep-lat\]](#).
- [20] J. Laiho and R. S. Van de Water, Pseudoscalar decay constants, light-quark masses, and B_K from mixed-action lattice QCD, *PoS LATTICE2011*, 293 (2011), [arXiv:1112.4861 \[hep-lat\]](#).

- [21] S. Durr, Z. Fodor, C. Hoelbling, S. D. Katz, S. Krieg, T. Kurth, L. Lellouch, T. Lippert, K. K. Szabo, and G. Vulvert (BMW), Lattice QCD at the physical point: light quark masses, *Phys. Lett. B* **701**, 265 (2011), [arXiv:1011.2403 \[hep-lat\]](#).
- [22] S. Durr, Z. Fodor, C. Hoelbling, S. D. Katz, S. Krieg, T. Kurth, L. Lellouch, T. Lippert, K. K. Szabo, and G. Vulvert (BMW), Lattice QCD at the physical point: Simulation and analysis details, *JHEP* **08**, 148, [arXiv:1011.2711 \[hep-lat\]](#).
- [23] A. Bazavov *et al.*, Staggered chiral perturbation theory in the two-flavor case and SU(2) analysis of the MILC data, *PoS LATTICE2010*, 083 (2010), [arXiv:1011.1792 \[hep-lat\]](#).
- [24] C. McNeile, C. T. H. Davies, E. Follana, K. Hornbostel, and G. P. Lepage, High-Precision c and b Masses, and QCD Coupling from Current-Current Correlators in Lattice and Continuum QCD, *Phys. Rev. D* **82**, 034512 (2010), [arXiv:1004.4285 \[hep-lat\]](#).
- [25] Y. Aoki *et al.* (RBC, UKQCD), Continuum Limit Physics from 2+1 Flavor Domain Wall QCD, *Phys. Rev. D* **83**, 074508 (2011), [arXiv:1011.0892 \[hep-lat\]](#).
- [26] C. T. H. Davies, C. McNeile, K. Y. Wong, E. Follana, R. Horgan, K. Hornbostel, G. P. Lepage, J. Shigemitsu, and H. Trottier, Precise Charm to Strange Mass Ratio and Light Quark Masses from Full Lattice QCD, *Phys. Rev. Lett.* **104**, 132003 (2010), [arXiv:0910.3102 \[hep-ph\]](#).
- [27] A. Bazavov *et al.* (MILC), MILC results for light pseudoscalars, *PoS CD09*, 007 (2009), [arXiv:0910.2966 \[hep-ph\]](#).
- [28] A. Bazavov *et al.* (MILC), Nonperturbative QCD Simulations with 2+1 Flavors of Improved Staggered Quarks, *Rev. Mod. Phys.* **82**, 1349 (2010), [arXiv:0903.3598 \[hep-lat\]](#).
- [29] Q. Mason, H. D. Trottier, R. Horgan, C. T. H. Davies, and G. P. Lepage (HPQCD), High-precision determination of the light-quark masses from realistic lattice QCD, *Phys. Rev. D* **73**, 114501 (2006), [arXiv:hep-ph/0511160](#).
- [30] C. Aubin, C. Bernard, C. E. DeTar, J. Osborn, S. Gottlieb, E. B. Gregory, D. Toussaint, U. M. Heller, J. E. Hetrick, and R. Sugar (MILC), Light pseudoscalar decay constants, quark masses, and low energy constants from three-flavor lattice QCD, *Phys. Rev. D* **70**, 114501 (2004), [arXiv:hep-lat/0407028](#).
- [31] C. Aubin *et al.* (HPQCD, MILC, UKQCD), First determination of the strange and light quark masses from full lattice QCD, *Phys. Rev. D* **70**, 031504 (2004), [arXiv:hep-lat/0405022](#).
- [32] M. Bruno, I. Campos, J. Koponen, C. Pena, D. Preti, A. Ramos, and A. Vladikas (ALPHA), Light and strange quark masses from $N_f = 2 + 1$ simulations with Wilson fermions, *PoS LATTICE2018*, 220 (2019), [arXiv:1903.04094 \[hep-lat\]](#).
- [33] N. Carrasco *et al.* (European Twisted Mass), Up, down, strange and charm quark masses with $N_f = 2+1+1$ twisted mass lattice QCD, *Nucl. Phys. B* **887**, 19 (2014), [arXiv:1403.4504 \[hep-lat\]](#).
- [34] A. Bazavov *et al.* (Fermilab Lattice, MILC, TUMQCD), Up-, down-, strange-, charm-, and bottom-quark masses from four-flavor lattice QCD, *Phys. Rev. D* **98**, 054517 (2018), [arXiv:1802.04248 \[hep-lat\]](#).
- [35] A. T. Lytle, C. T. H. Davies, D. Hatton, G. P. Lepage, and C. Sturm (HPQCD), Determination of quark masses from $n_f = 4$ lattice QCD and the RI-SMOM intermediate scheme, *Phys. Rev. D* **98**, 014513 (2018), [arXiv:1805.06225 \[hep-lat\]](#).
- [36] B. Chakraborty, C. T. H. Davies, B. Galloway, P. Knecht, J. Koponen, G. C. Donald, R. J. Dowdall, G. P. Lepage, and C. McNeile, High-precision quark masses and QCD coupling from $n_f = 4$ lattice QCD, *Phys. Rev. D* **91**, 054508 (2015), [arXiv:1408.4169 \[hep-lat\]](#).
- [37] A. Bazavov *et al.*, B - and D -meson leptonic decay constants from four-flavor lattice QCD, *Phys. Rev. D* **98**, 074512 (2018), [arXiv:1712.09262 \[hep-lat\]](#).
- [38] A. Bazavov *et al.* (Fermilab Lattice, MILC), Charmed and Light Pseudoscalar Meson Decay Constants from Four-Flavor Lattice QCD with Physical Light Quarks, *Phys. Rev. D* **90**, 074509 (2014), [arXiv:1407.3772 \[hep-lat\]](#).
- [39] C. Alexandrou *et al.* (Extended Twisted Mass), Ratio of kaon and pion leptonic decay constants with $N_f=2+1+1$ Wilson-clover twisted-mass fermions, *Phys. Rev. D* **104**, 074520 (2021), [arXiv:2104.06747 \[hep-lat\]](#).
- [40] N. Miller *et al.*, F_K/F_π from Möbius Domain-Wall fermions solved on gradient-flowed HISQ ensembles, *Phys. Rev. D* **102**, 034507 (2020), [arXiv:2005.04795 \[hep-lat\]](#).
- [41] N. Carrasco *et al.*, Leptonic decay constants f_K , f_D , and f_{D_s} with $N_f = 2 + 1 + 1$ twisted-mass lattice QCD, *Phys. Rev. D* **91**, 054507 (2015), [arXiv:1411.7908 \[hep-lat\]](#).
- [42] P. Dimopoulos, R. Frezzotti, P. Lami, V. Lubicz, E. Picca, L. Riggio, G. C. Rossi, F. Sanfilippo, S. Simula, and C. Tarantino, Pseudoscalar decay constants f_K/f_π , f_D and f_{D_s} with $N_f = 2 + 1 + 1$ ETMC configurations, *PoS LATTICE2013*, 314 (2014), [arXiv:1311.3080 \[hep-lat\]](#).
- [43] R. J. Dowdall, C. T. H. Davies, G. P. Lepage, and C. McNeile, V_{us} from π and K decay constants in full lattice QCD with physical u, d, s and c quarks, *Phys. Rev. D* **88**, 074504 (2013), [arXiv:1303.1670 \[hep-lat\]](#).
- [44] A. Bazavov *et al.* (MILC), Leptonic Decay-Constant Ratio f_{K^+}/f_{π^+} from Lattice QCD with Physical Light Quarks, *Phys. Rev. Lett.* **110**, 172003 (2013), [arXiv:1301.5855 \[hep-ph\]](#).
- [45] A. Bazavov *et al.* (MILC), Properties of light pseudoscalars from lattice QCD with HISQ ensembles, *PoS LATTICE2011*, 107 (2011), [arXiv:1111.4314 \[hep-lat\]](#).
- [46] F. Farchioni, G. Herdoiza, K. Jansen, A. Nube, M. Petschlies, and C. Urbach, Pseudoscalar decay constants from $N_f=2+1+1$ twisted mass lattice QCD, *PoS LATTICE2010*, 128 (2010), [arXiv:1012.0200 \[hep-lat\]](#).
- [47] V. G. Bornyakov, R. Horsley, Y. Nakamura, H. Perlt, D. Pleiter, P. E. L. Rakow, G. Schierholz, A. Schiller, H. Stüben, and J. M. Zanotti (QCDSF-UKQCD), Flavour breaking effects in the pseudoscalar meson decay constants, *Phys. Lett. B* **767**, 366 (2017), [arXiv:1612.04798 \[hep-lat\]](#).
- [48] S. Dürr *et al.*, Leptonic decay-constant ratio f_K/f_π from lattice QCD using 2+1 clover-improved fermion flavors with 2-HEX smearing, *Phys. Rev. D* **95**, 054513 (2017), [arXiv:1601.05998 \[hep-lat\]](#).
- [49] E. E. Scholz and S. Durr, Leptonic decay-constant ratio f_K/f_π from clover-improved $N_f = 2 + 1$ QCD, *PoS LATTICE2016*, 283 (2016), [arXiv:1610.00932 \[hep-lat\]](#).
- [50] A. Bazavov *et al.* (MILC), Results for light pseudoscalar mesons, *PoS LATTICE2010*, 074 (2010), [arXiv:1012.0868 \[hep-lat\]](#).

- [51] S. Durr, Z. Fodor, C. Hoelbling, S. D. Katz, S. Krieg, T. Kurth, L. Lellouch, T. Lippert, A. Ramos, and K. K. Szabo (BMW), The ratio $FK/F\pi$ in QCD, *Phys. Rev. D* **81**, 054507 (2010), [arXiv:1001.4692 \[hep-lat\]](#).
- [52] C. Aubin, J. Laiho, and R. S. Van de Water, Light Pseudoscalar Meson Masses and Decay Constants from Mixed Action Lattice QCD, *PoS LATTICE2008*, 105 (2008), [arXiv:0810.4328 \[hep-lat\]](#).
- [53] E. Follana, C. T. H. Davies, G. P. Lepage, and J. Shigemitsu (HPQCD, UKQCD), High Precision determination of the π , K , D and $D(s)$ decay constants from lattice QCD, *Phys. Rev. Lett.* **100**, 062002 (2008), [arXiv:0706.1726 \[hep-lat\]](#).
- [54] B. Fahy, G. Cossu, S. Hashimoto, T. Kaneko, J. Noaki, and M. Tomii (JLQCD), Decay constants and spectroscopy of mesons in lattice QCD using domain-wall fermions, *PoS LATTICE2015*, 074 (2016), [arXiv:1512.08599 \[hep-lat\]](#).
- [55] J. Liang, A. Alexandru, Y.-J. Bi, T. Draper, K.-F. Liu, and Y.-B. Yang (χ QCD), Detecting the flavor content of the vacuum using the Dirac operator spectrum, *Phys. Rev. D* **110**, 094513 (2024), [arXiv:2102.05380 \[hep-lat\]](#).
- [56] C. Alexandrou, A. Athenodorou, K. Cichy, M. Constantinou, D. P. Horkel, K. Jansen, G. Koutsou, and C. Larkin, Topological susceptibility from twisted mass fermions using spectral projectors and the gradient flow, *Phys. Rev. D* **97**, 074503 (2018), [arXiv:1709.06596 \[hep-lat\]](#).
- [57] K. Cichy, E. Garcia-Ramos, and K. Jansen, Chiral condensate from the twisted mass Dirac operator spectrum, *JHEP* **10**, 175, [arXiv:1303.1954 \[hep-lat\]](#).
- [58] S. Aoki, G. Cossu, H. Fukaya, S. Hashimoto, and T. Kaneko (JLQCD), Topological susceptibility of QCD with dynamical Möbius domain-wall fermions, *PTEP* **2018**, 043B07 (2018), [arXiv:1705.10906 \[hep-lat\]](#).
- [59] P. A. Boyle *et al.*, Low energy constants of $SU(2)$ partially quenched chiral perturbation theory from $N_f=2+1$ domain wall QCD, *Phys. Rev. D* **93**, 054502 (2016), [arXiv:1511.01950 \[hep-lat\]](#).
- [60] S. Dürr *et al.* (BMW), Lattice QCD at the physical point meets $SU(2)$ chiral perturbation theory, *Phys. Rev. D* **90**, 114504 (2014), [arXiv:1310.3626 \[hep-lat\]](#).
- [61] S. Borsanyi, S. Durr, Z. Fodor, S. Krieg, A. Schafer, E. E. Scholz, and K. K. Szabo, $SU(2)$ chiral perturbation theory low-energy constants from $2+1$ flavor staggered lattice simulations, *Phys. Rev. D* **88**, 014513 (2013), [arXiv:1205.0788 \[hep-lat\]](#).
- [62] G. P. Engel, L. Giusti, S. Lottini, and R. Sommer, Spectral density of the Dirac operator in two-flavor QCD, *Phys. Rev. D* **91**, 054505 (2015), [arXiv:1411.6386 \[hep-lat\]](#).
- [63] B. B. Brandt, A. Jüttner, and H. Wittig, The pion vector form factor from lattice QCD and NNLO chiral perturbation theory, *JHEP* **11**, 034, [arXiv:1306.2916 \[hep-lat\]](#).
- [64] F. Burger, V. Lubicz, M. Müller-Preussker, S. Simula, and C. Urbach, Quark mass and chiral condensate from the Wilson twisted mass lattice quark propagator, *Phys. Rev. D* **87**, 034514 (2013), [arXiv:1210.0838 \[hep-lat\]](#).
- [65] R. Baron *et al.* (ETM), Light Meson Physics from Maximally Twisted Mass Lattice QCD, *JHEP* **08**, 097, [arXiv:0911.5061 \[hep-lat\]](#).
- [66] R. Frezzotti, V. Lubicz, and S. Simula (ETM), Electromagnetic form factor of the pion from twisted-mass lattice QCD at $N(f) = 2$, *Phys. Rev. D* **79**, 074506 (2009), [arXiv:0812.4042 \[hep-lat\]](#).
- [67] R. Baron *et al.* (ETM), Light hadrons from $N_f=2+1+1$ dynamical twisted mass fermions, *PoS LATTICE2010*, 123 (2010), [arXiv:1101.0518 \[hep-lat\]](#).
- [68] S. R. Beane, W. Detmold, P. M. Junnarkar, T. C. Luu, K. Orginos, A. Parreno, M. J. Savage, A. Torok, and A. Walker-Loud, $SU(2)$ Low-Energy Constants from Mixed-Action Lattice QCD, *Phys. Rev. D* **86**, 094509 (2012), [arXiv:1108.1380 \[hep-lat\]](#).
- [69] R. Horsley, Y. Nakamura, A. Nobile, P. E. L. Rakow, G. Schierholz, and J. M. Zanotti, Nucleon axial charge and pion decay constant from two-flavor lattice QCD, *Phys. Lett. B* **732**, 41 (2014), [arXiv:1302.2233 \[hep-lat\]](#).
- [70] G. Colangelo and S. Durr, The Pion mass in finite volume, *Eur. Phys. J. C* **33**, 543 (2004), [arXiv:hep-lat/0311023](#).
- [71] V. Gülpers, G. von Hippel, and H. Wittig, The scalar radius of the pion from Lattice QCD in the continuum limit, *Eur. Phys. J. A* **51**, 158 (2015), [arXiv:1507.01749 \[hep-lat\]](#).
- [72] S. Aoki *et al.* (JLQCD, TWQCD), Pion form factors from two-flavor lattice QCD with exact chiral symmetry, *Phys. Rev. D* **80**, 034508 (2009), [arXiv:0905.2465 \[hep-lat\]](#).
- [73] S. Navas *et al.* (Particle Data Group), Review of particle physics, *Phys. Rev. D* **110**, 030001 (2024).
- [74] X. Jiang, C. Shi, Y. Chen, M. Gong, and Y.-B. Yang, Use QUDA for lattice QCD calculation with Python, (2024), [arXiv:2411.08461 \[hep-lat\]](#).
- [75] M. A. Clark, R. Babich, K. Barros, R. C. Brower, and C. Rebbi (QUDA), Solving Lattice QCD systems of equations using mixed precision solvers on GPUs, *Comput. Phys. Commun.* **181**, 1517 (2010), [arXiv:0911.3191 \[hep-lat\]](#).
- [76] R. Babich, M. A. Clark, B. Joo, G. Shi, R. C. Brower, and S. Gottlieb (QUDA), Scaling lattice QCD beyond 100 GPUs, in *International Conference for High Performance Computing, Networking, Storage and Analysis* (2011) [arXiv:1109.2935 \[hep-lat\]](#).
- [77] M. A. Clark, B. Joó, A. Strelchenko, M. Cheng, A. Gambhir, and R. C. Brower (QUDA), Accelerating lattice QCD multigrid on GPUs using fine-grained parallelization, in *International Conference for High Performance Computing, Networking, Storage and Analysis* (2016) [arXiv:1612.07873 \[hep-lat\]](#).
- [78] Y.-J. Bi, Y. Xiao, W.-Y. Guo, M. Gong, P. Sun, S. Xu, and Y.-B. Yang, Lattice QCD package GWU-code and QUDA with HIP, *PoS LATTICE2019*, 286 (2020), [arXiv:2001.05706 \[hep-lat\]](#).

APPENDIX

Table V lists the tadpole factor v_0 (derived from smeared links for the clover term) and the tuned dimensionless valence clover masses $\tilde{m}_{l,s,c}^v$. These masses are tuned to reproduce, respectively, the unitary pion mass, the physical η_s mass (689.89(49) MeV), and the QED-subtracted D_s mass (1966.7(1.5) MeV). For completeness, the table also includes the basic information for the HISQ ensembles, which are shown separately in Table II.

TABLE V. Summary table on the lattice spacing, $\tilde{L}^3 \times \tilde{T}$, $m_\pi L$ and m_{π,η_s,η_c} (in MeV) of the CLQCD ensembles with HISQ fermion [3].

Ensemble	a (fm)	$\tilde{L}^3 \times \tilde{T}$	$m_\pi L$	m_π	m_{η_s}	m_{η_c}	v_0	\tilde{m}_l^v	\tilde{m}_s^v	\tilde{m}_c^v
c24P31s		$24^3 \times 48$	4.13	313(2)	745(3)	2.973(12)	0.9636	-0.1946	-0.1557	
c24P31		$24^3 \times 48$	4.07	309(2)	687(3)	2.972(12)	0.9636	-0.1946	-0.1554	0.530
c32P31		$32^3 \times 48$	5.44	310(1)	686(3)	2.972(12)	0.9636	-0.1945	-0.1553	
c24P22	0.1084(4)	$24^3 \times 48$	2.94	223(2)	685(3)	2.970(12)	0.9636	-0.1991	-0.1552	
c32P22		$32^3 \times 48$	3.87	220(1)	684(3)	2.970(12)	0.9636	-0.1991	-0.1544	
c48P13		$48^3 \times 48$	3.53	134(1)	683(3)	2.970(12)	0.9636	-0.2016	-0.1540	
e32P31	0.0867(4)	$32^3 \times 64$	4.41	313(2)	694(3)	3.015(13)	0.9678	-0.1645	-0.1352	
g32P32		$32^3 \times 64$	3.65	317(3)	692(3)	2.981(13)	0.9707	-0.1455	-0.1231	0.240
g48P31	0.0710(3)	$48^3 \times 64$	5.38	311(2)	691(3)	2.983(13)	0.9707	-0.1457	-0.1231	
h48P31	0.0473(3)	$48^3 \times 96$	3.60	313(3)	692(5)	2.947(19)	0.9754	-0.1173	-0.1035	
x24P31	0.1114(6)	$24^3 \times 48$	4.35	321(2)	711(4)	–	0.9605	–	-0.1755	0.541
y24P31	0.1116(6)	$24^3 \times 48$	4.22	311(2)	688(4)	–	0.9623	-0.2038	-0.1540	0.563
z24P31	0.1128(7)	$24^3 \times 48$	4.35	317(2)	704(4)	–	0.9663	–	-0.1353	0.610

Table VI lists the renormalization constants $Z_{S/P/T}$ matched to the $\overline{\text{MS}}$ scheme at 2 GeV, obtained via intermediate matching in the RI/MOM ($\omega = 0$) and SMOM ($\omega = 1$) schemes. The ratios Z_X/Z_V of the current $X \equiv \bar{q}\Gamma_X q$ are determined from the vertex functions

$$\frac{Z_X(\mu^{\text{RI}}, \omega)}{Z_V} = \frac{\frac{1}{48} \text{Tr}[\Lambda_V(\mu^{\text{RI}}, \omega) \gamma_\mu]}{\frac{1}{c_X} \text{Tr}[\Lambda_X^\mu(\mu^{\text{RI}}, \omega) \Gamma_X]}, \quad (14)$$

where $\Lambda_O(\mu^{\text{RI}}, \omega) = S^{-1}(p_1) G_O(p_1, p_2) S^{-1}(p_2)$, evaluated at kinematics satisfying $p_1^2 = p_2^2 = (\mu^{\text{RI}})^2$ and $(p_1 - p_2)^2 = \omega p_1^2$, and c_X is a constant dependent on the corresponding current. From the table, one can observe that the differences between the MOM ($\omega = 0$) and SMOM ($\omega = 1$) results diminish as the lattice spacing decreases.

TABLE VI. Renormalization constants in $\overline{\text{MS}}$ 2 GeV (if applicable) through the RI/MOM and SMOM schemes. The values of Z_V are obtained from the pion matrix element and then the same in both the schemes.

Ensemble	Z_V	Z_A/Z_V		Z_S/Z_V		Z_P/Z_V		Z_T/Z_V	
		MOM	SMOM	MOM	SMOM	MOM	SMOM	MOM	SMOM
c24P31s	0.8476(2)	1.064(2)	1.017(3)	1.201(06)(38)	0.986(05)(10)	0.969(17)(28)	0.941(03)(10)	1.074(01)(05)	1.070(02)(04)
c24P31	0.8476(2)	1.064(2)	1.017(3)	1.204(05)(35)	0.978(06)(10)	0.995(19)(28)	0.945(04)(10)	1.076(01)(05)	1.071(02)(04)
c32P31	0.8479(1)	1.060(2)	1.015(2)	1.199(05)(35)	0.991(03)(11)	0.974(17)(27)	0.937(03)(10)	1.072(01)(05)	1.069(01)(04)
c24P22	0.8478(2)	1.061(2)	1.018(2)	1.193(04)(37)	0.985(05)(10)	0.965(14)(28)	0.943(04)(10)	1.074(01)(05)	1.071(02)(04)
c32P22	0.8481(1)	1.062(2)	1.022(2)	1.202(04)(36)	0.994(03)(11)	0.986(16)(27)	0.934(03)(10)	1.072(01)(05)	1.074(01)(04)
c48P13	0.8484(1)	1.062(1)	1.016(1)	1.200(03)(35)	0.989(03)(11)	0.961(09)(26)	0.942(02)(10)	1.073(01)(05)	1.068(01)(04)
e32P31	0.8720(1)	1.049(1)	1.016(1)	1.097(02)(23)	0.939(02)(08)	0.919(07)(19)	0.897(01)(08)	1.085(01)(04)	1.085(01)(04)
g32P32	0.8872(2)	1.042(1)	1.013(1)	1.018(04)(21)	0.898(02)(07)	0.864(10)(17)	0.865(01)(07)	1.098(01)(04)	1.097(01)(04)
g48P31	0.8876(1)	1.037(1)	1.011(1)	1.016(02)(23)	0.902(01)(08)	0.876(06)(17)	0.873(01)(07)	1.094(01)(04)	1.093(01)(04)
h48P31	0.9108(1)	1.027(1)	1.010(1)	0.912(03)(11)	0.836(01)(07)	0.813(03)(10)	0.810(01)(06)	1.118(01)(03)	1.119(01)(04)
y24P31	0.8407(3)	1.063(2)	1.019(4)	1.212(11)(35)	0.994(07)(11)	0.966(34)(28)	0.949(03)(10)	1.072(02)(05)	1.069(02)(04)

Figure 4 shows the ratio Z_A/Z_V calculated in the MOM (data points) and SMOM (bands) schemes at various lattice spacings a , plotted as a function of $a^2(\mu^{\text{RI}})^2$. This quantity characterizes the additive chiral symmetry breaking of the clover fermion action. Comparing the $N_f = 2 + 1$ unitary clover case (CL@CL, left panel) with the $N_f = 2 + 1 + 1$ clover-on-HISQ case (CL@HI, right panel), the extrapolated values of Z_A/Z_V to $a^2(\mu^{\text{RI}})^2 \rightarrow 0$ —obtained from a polynomial fit to data with $\mu^{\text{RI}} \geq 3$ GeV—are similar at comparable lattice spacings.

In contrast, the deviation of Z_S/Z_P from 1 is significantly larger in the CL@CL case than in the CL@HI case. As shown in Fig. 5, the difference is more pronounced at coarser lattice spacings. The suppression of $Z_S/Z_P - 1$ in

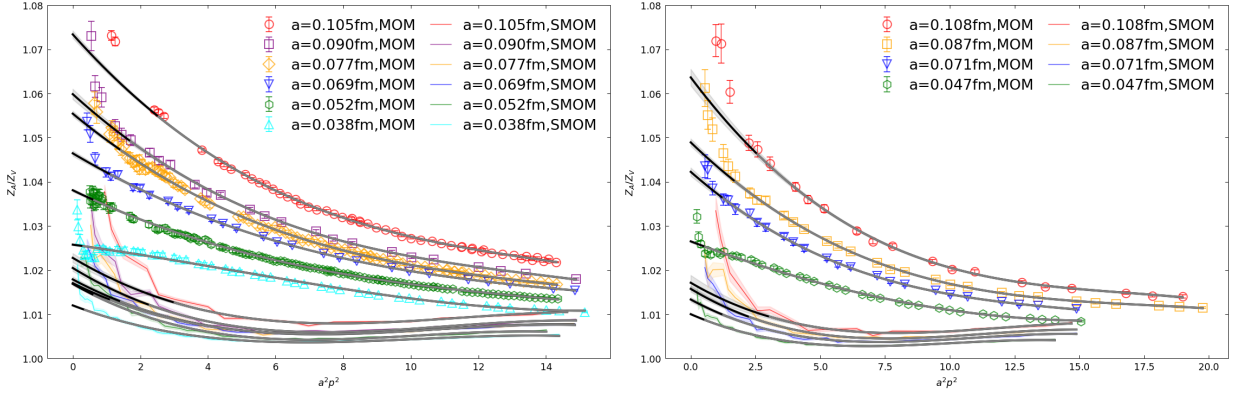


FIG. 4. $a^2(\mu^{\text{RI}})^2$ dependence of Z_A/Z_V at different lattice spacing using the $N_f = 2 + 1$ unitary clover setup (left panel) and the $N_f = 2 + 1 + 1$ clover on HISQ setup (right panel).

the CL@HI setup likely originates from the smaller tadpole-improved bare coupling compared to the CL@CL case, a point that merits further investigation.

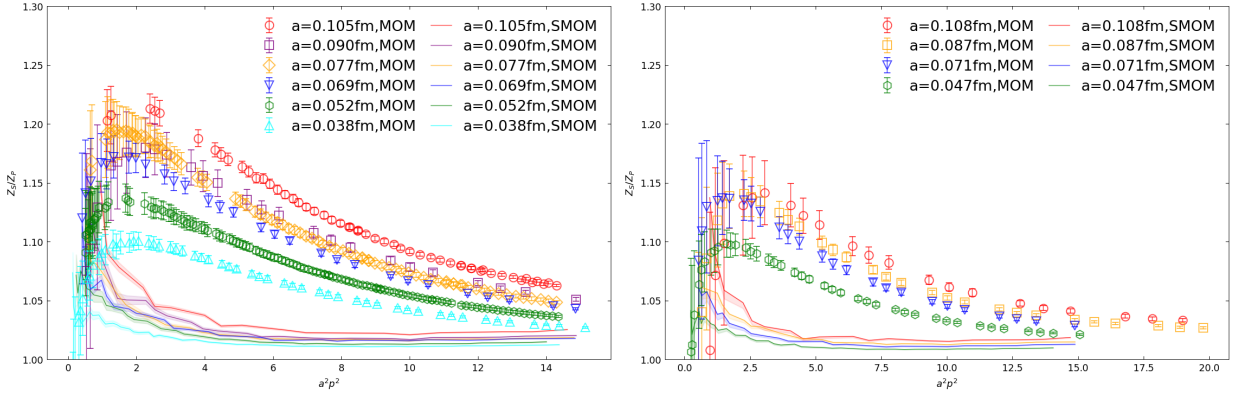


FIG. 5. Similar to Fig. 4 but for Z_S/Z_P .